A THREE-PHASE ZVS PWM DC/DC CONVERTER ASSOCIATED WITH A DOUBLE-WYE CONNECTED RECTIFIER, DELTA PRIMARY

Demercil S. Oliveira Jr. and Fernando L. M. Antunes
Group of Energy Processing and Control
Federal University of Ceará
demercil@dee.ufc.br, fantunes@dee.ufc.br

***Abstract* – This paper presents the theoretical analysis of the three-phase ZVS PWM dc/dc converter associated with a double wye connected rectifier, delta primary, using a special switching scheme in order to maintain equilibrium among the currents through the output filters. The operating stages are described and the dynamic model of the converter is obtained. Simulation and experimental results of a 6kW prototype are presented.**

***Keywords* – three-phase, dc/dc converter, ZVS commutation.**

I. INTRODUCTION

The main topology used in high power dc/dc conversion is the ZVS PWM Full Bridge converter with phase-shift control [1][2]. However, at higher power levels, the components face several stresses. An interesting alternative was proposed by Ziogas in [3]. It uses a three-phase inverter coupled to a three-phase high frequency transformer and to a three-phase high frequency rectifier. The resulting advantages consist of the increase of the input and output current frequency by a factor of three compared to the full-bridge converter, lower rms current through power components and reduction of the cores. Although it presents satisfactory advantages, soft commutation has not been achieved, which limits the switching frequency and the power density.

Then, the use of asymmetrical duty cycle [4] in the three-phase dc/dc converter was proposed in [5], in order to provide ZVS commutation of all switches for a wide load range, as shown in Fig. 1.

Nevertheless, analogously to the full-bridge converter, the resulting topology suffers higher conduction losses in the rectifier stage, since two series diodes conduct the load current. Therefore, the association of a three-phase dc/dc converter and a three-phase high efficiency rectifier seems to be an optimal arrangement for applications that demand high current levels and low output voltages. In [6] (Fig. 2), the use of a three-phase version of the hybridge rectifier improved efficiency in about 2%. However, there is a natural increase in the output inductors volume. Besides, disequilibrium among the currents through the output inductors causes the output inductors to be overdesigned, implying even more increased volume.

II. THE PROPOSED THREE-PHASE RECTIFIER

A. Proposed Topology

In order to overcome the efficiency limit imposed by the full-bridge rectifier used in [5], without causing the increase of the output inductors [6], this paper proposes the use of double-wye connection in the transformer [7]. This rectifier is formed by six diodes and two inductors, as shown in Fig. 3. The output inductors act as an interphase transformer as well as an output filter. The use of two inductors does not increase volume as in the Full-Bridge rectifier.

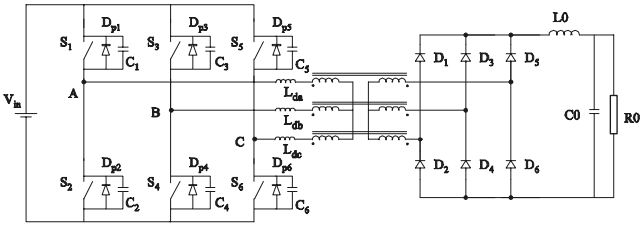

Fig. 1 – Association with the three-phase full-bridge rectifier [5].

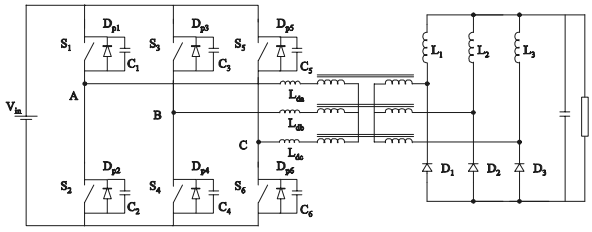

Fig. 2 – Association with the hybridge rectifier [6].

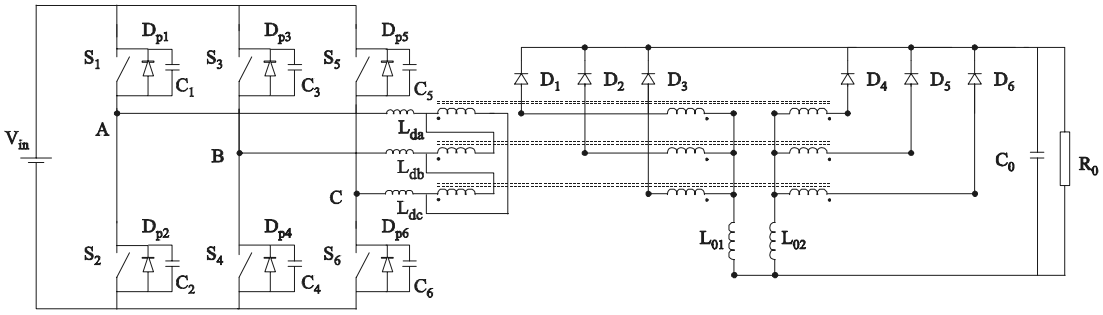

Fig. 3 – Three-phase ZVS dc/dc converter associated with the hybridge rectifier.

TABLE I
Operating Stages

	First Stage	Second Stage	Third Stage	Fourth Stage
$i_A(t)$	$-\frac{I_L}{2}-\frac{1}{3}\frac{V_{in}}{L_d}t$	$-I_L+\frac{1}{6}\frac{V_{in}}{L_d}t$	$-\frac{I_L}{2}$	$-\frac{I_L}{2}$
$i_B(t)$	$I_L-\frac{1}{3}\frac{V_{in}}{L_d}t$	$\frac{I_L}{2}-\frac{1}{3}\frac{V_{in}}{L_d}t$	$-\frac{I_L}{2}$	$-\frac{I_L}{2}$
$i_C(t)$	$-\frac{I_L}{2}+\frac{2}{3}\frac{V_{in}}{L_d}t$	$\frac{I_L}{2}+\frac{1}{6}\frac{V_{in}}{L_d}t$	I_L	I_L
$i_{Lpa}(t)$	I_f	$-I_f+\frac{1}{6}\frac{V_{in}}{L_d}t$	0	0
$i_{Lpb}(t)$	$I_f-\frac{1}{3}\frac{V_{in}}{L_d}t$	$-\frac{1}{6}\frac{V_{in}}{L_d}t$	$-I_f$	$-I_f$
$i_{Lpc}(t)$	$\frac{1}{3}\frac{V_{in}}{L_d}t$	I_f	I_f	I_f
Δt	$\frac{3L_d}{V_{in}}I_f$	$\frac{6L_d}{V_{in}}I_f$	$\frac{DT_s}{3}-\Delta t_1-\Delta t_2$	$\frac{(1-D)T_s}{3}$
V_{f1}	0	V_{in}	V_{in}	0
V_{f2}	0	$\frac{V_{in}}{2}$	V_{in}	0

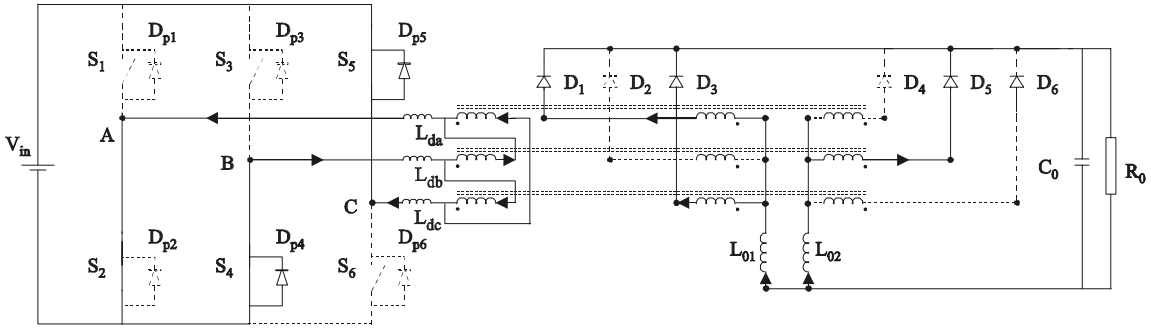

Fig. 4 – First stage.

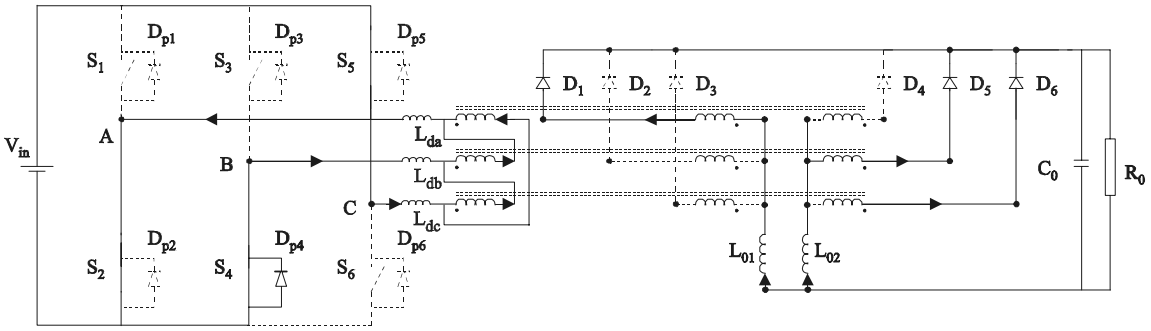

Fig. 5 – Second stage.

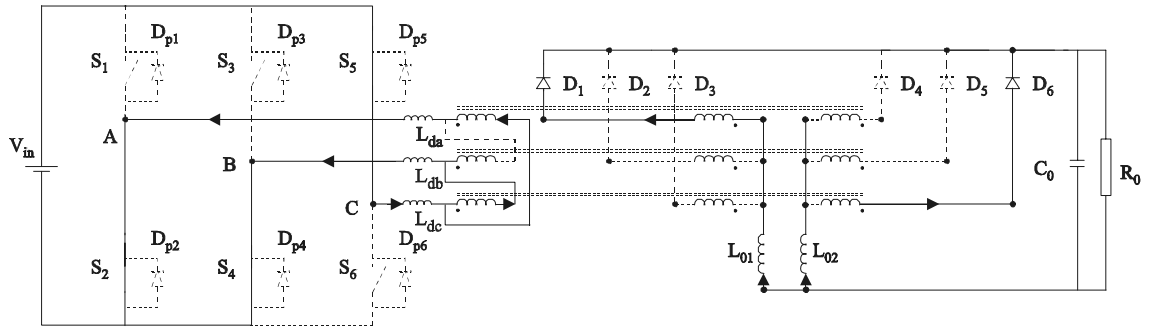

Fig. 6 – Third stage.

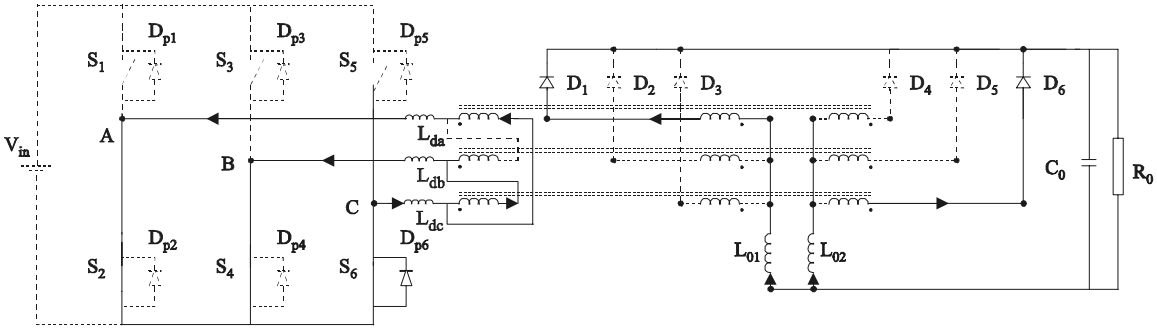

Fig. 7 – Fourth stage.

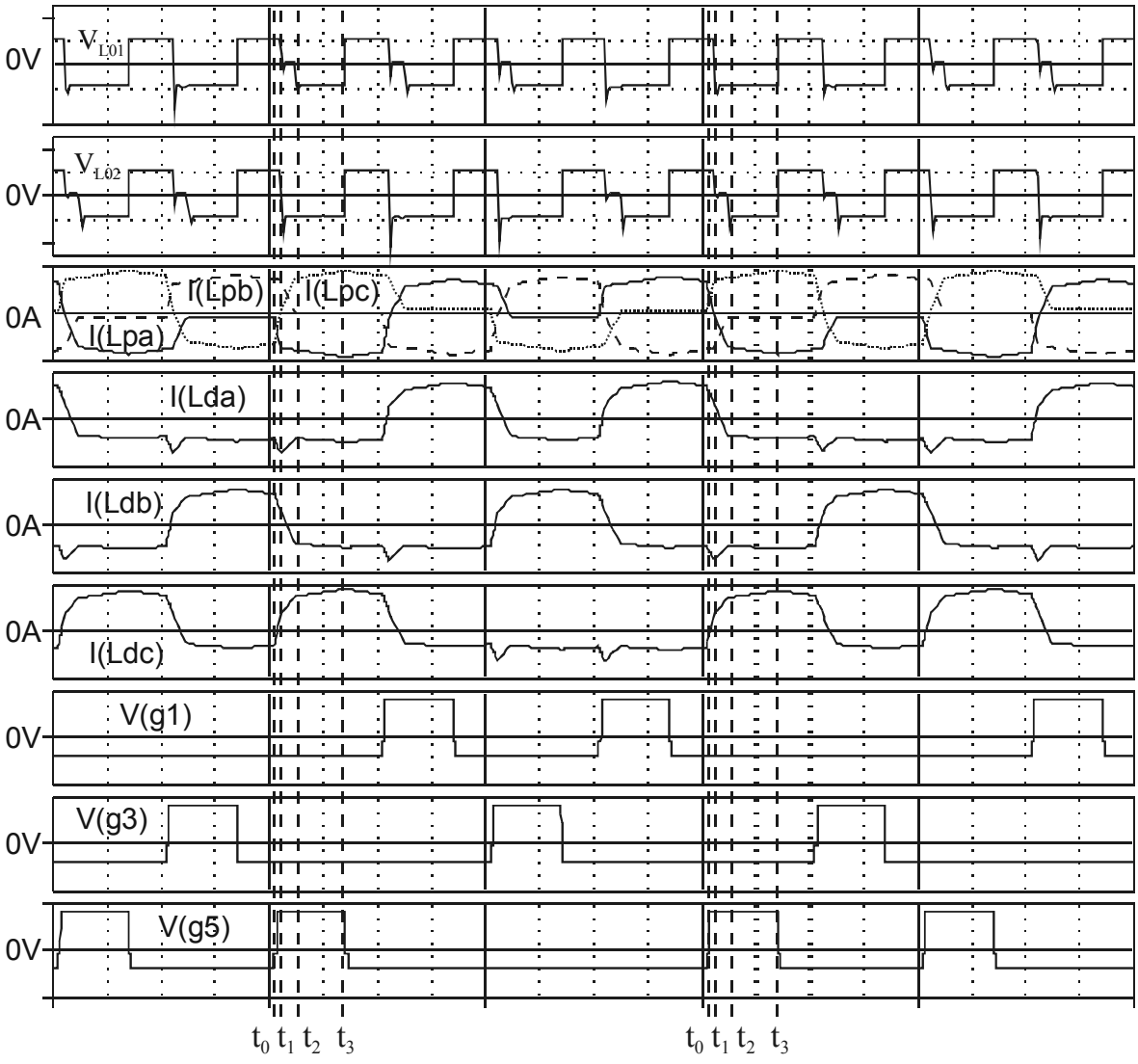

Fig. 8 – Main waveforms.

B. Operating Stages

The equations representing line and phase currents (i_A, i_B, i_C and i_{Lpa}, i_{Lpb}, i_{Lpc}), voltages applied to the output filters (V_{f1} and V_{f2}) and the time intervals of each operating stage (Δt_i), are presented in Table I. The operating stages are described considering ideal transformer and semiconductors. Besides, the duty cycle is applied to switches S_1, S_3 and S_5.

First Stage [t_0, t_1]: This stage begins when switch S_5 is turned on. All line and phase currents have linear behavior, according to Fig. 8. At the end of this stage, diode D_3 is reverse biased and diode D_6 is forward biased.

Second Stage [t_1, t_2]: As i_{Lpa} has reached its maximum value, i_{Lpb} and i_{Lpc} vary linearly, causing the linear transition in the line currents, as in Fig. 8. At the end of this stage, diode D_5 is reverse biased and diode D_6 conducts i_{L02}. This additional transition stage is responsible for a disequilibrium between output currents i_{L01} and i_{L02}.

Third Stage [t_2, t_3]: At the end of the linear transitions, energy transference begins, until the end of duty cycle.

Fourth Stage [t_3, t_4]: This stage begins when the PWM controller determines the end of the duty cycle. The behavior of the circuit is shown in Fig 7, what characterizes a freewheeling stage.

From the aforementioned analysis, one can obtain the average voltage applied to each output filter as:

$$V_{f1+} = V_{in}\left[D - 9\frac{L_d}{V_{in}T_s}I_f\right] \quad (1)$$

$$V_{f2+} = V_{in}\left[D - 18\frac{L_d}{V_{in}T_s}I_f\right] \quad (2)$$

The difference between the average voltages, verified in the second stage, causes disequilibrium in the currents through inductors L_{01} and L_{02}. Then, as described in [8], conventional switching schemes can not provide output voltage control of this converter.

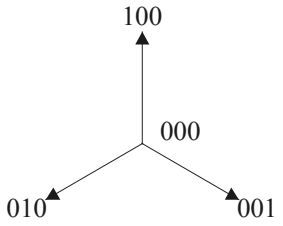

Fig. 9 – Vectors in each operating mode.

C. PN Modulation

According to [5], in MINCIM mode, the possible vectors are shown in Fig. 9 (D<0.33), where "1" and "0" correspond to the on and off states of switch S_i, respectively. The expressions in Table I are obtained using clockwise sequence (100 – 000 – 010 – 000 – 001). However, for anticlockwise sequence, $V_{f1}=V_{in}/2$ and $V_{f2}=V_{in}$, in the second stage. As a result, the average voltages applied to each output filter, for anticlockwise sequence, are given by:

$$V_{f1-} = V_{in}\left[D - 18\frac{L_d}{V_{in}T_s}I_f\right] \quad (3)$$

$$V_{f2-} = V_{in}\left[D - 9\frac{L_d}{V_{in}T_s}I_f\right] \quad (4)$$

Then, a new switching scheme, named "PN Modulation" is proposed, which consists of the use of clockwise and anticlockwise sequences in an alternate way (100 –010 – 001 – 100 – 001 – 010). Therefore, the average voltage applied to each output filter for two switching periods are given by (5), as the disequilibrium between the currents through the output inductors is minimized, enabling output voltage control with pulse width modulation.

$$V_{f1} = V_{f2} = V_{in}\left[D - \frac{27}{2}\frac{L_d}{V_{in}T_s}I_f\right] \quad (5)$$

D. Unbalance Considerations

A disequilibrium between the currents through the output inductors causes dc unbalance and consequently core saturation, if three uncoupled transformers are used. Then, an optimum equilibrium must be provided as obtained in the PN modulation.

In a secondary double-wye connection, without interphase inductors, there is ac unbalance, which is not acceptable, since it promotes an ac flux path outside of the core. The presence of interphase inductors mitigates such unbalance and reduces rms currents through the secondary windings, as well as through output diodes D_1, D_2, …, D_6, because it increases the conduction angle.

III. DYNAMICAL ANALISYS

A. NonLinear Model

From the operating stages, one can obtain the state space equation (6), where $L=L_{01}/2$ and $i_L = i_{L01} + i_{L02}$.

$$\begin{bmatrix}\dot{i}_L \\ \dot{v}_C\end{bmatrix} = \begin{bmatrix}-\frac{1}{L}\cdot\frac{R\cdot r_{SE}}{R+r_{SE}} & -\frac{1}{L}\cdot\frac{R}{R+r_{SE}} \\ \frac{1}{C}\cdot\frac{R}{R+r_{SE}} & -\frac{1}{C}\cdot\frac{1}{R+r_{SE}}\end{bmatrix}\begin{bmatrix}i_L \\ v_C\end{bmatrix} + \begin{bmatrix}\frac{q(t)}{L} \\ 0\end{bmatrix}V_{in} \quad (6)$$

The switching function $q(t)$ is defined in (7), where n≥0:

$$q(t) = \begin{cases}0, \text{ if stage 4n+1 or 4n+4} \\ 3/4, \text{ if stage 4n+2} \\ 1, \text{ if stage 4n+3}\end{cases} \quad (7)$$

The equilibrium points are given by (8), and the eigenvalues can be real or complex, depending on the parameters of the circuit.

$$\bar{X} = \begin{bmatrix}\frac{1}{R} \\ 1\end{bmatrix}V_{in}q(t) \quad (8)$$

Defining the average effective duty cycle in (9), where R_d is the duty cycle loss caused by the series inductance $L_d=L_{da}=L_{db}=L_{dc}$, the nonlinear model, in the average state space, can be obtained in (11).

$$d = D_{ef}(t) = \langle q(t)\rangle_{T_s} - \frac{R_d}{V_{in}}\langle i_L(t)\rangle_{T_s} \quad (9)$$

$$R_d = \frac{27}{4}f_s L_d \quad (10)$$

$$\begin{bmatrix}\dot{i}_L \\ \dot{v}_C\end{bmatrix} = \begin{bmatrix}-\frac{1}{L}\cdot\frac{R\cdot r_{SE}}{R+r_{SE}} & -\frac{1}{L}\cdot\frac{R}{R+r_{SE}} \\ \frac{1}{C}\cdot\frac{R}{R+r_{SE}} & -\frac{1}{C}\cdot\frac{1}{R+r_{SE}}\end{bmatrix}\begin{bmatrix}i_L \\ v_C\end{bmatrix} + \begin{bmatrix}\frac{d}{L} \\ 0\end{bmatrix}V_{in} \quad (11)$$

By equaling its (11) to zero, the equilibrium points of the nonlinear model can be obtained.

$$\bar{X} = \begin{bmatrix}\frac{1}{R+R_d} \\ \frac{R}{R+R_d}\end{bmatrix}d\cdot V_{in} \quad (12)$$

B. Linearization

Defining the equilibrium points (I_L, V_C, D, V_{in}, R), and using the Jacobian concept, the linearized average state space equation can be found in (13).

$$\begin{bmatrix} \dot{i}_L \\ \dot{v}_C \end{bmatrix} = \begin{bmatrix} -\frac{1}{L}\cdot\frac{R\cdot r_{SE}}{R+r_{SE}} & -\frac{1}{L}\cdot\frac{R}{R+r_{SE}} \\ \frac{1}{C}\cdot\frac{R}{R+r_{SE}} & -\frac{1}{C}\cdot\frac{1}{R+r_{SE}} \end{bmatrix} \begin{bmatrix} i_L \\ v_C \end{bmatrix} + \\ + \begin{bmatrix} \frac{V_{in}}{L} & \frac{D}{L} & \frac{-dV_{in}r_{SE}}{(R+r_{SE})(R+r_{SE})} \\ 0 & 0 & \frac{dV_{in}}{(R+r_{SE})(R+r_{SE})} \end{bmatrix} \cdot \begin{bmatrix} \Delta d \\ \Delta v_{in} \\ \Delta r \end{bmatrix} \quad (13)$$

Solving the transference matrix, one can obtain the complete dynamic transfer functions of the three-phase dc/dc converter.

IV. EXPERIMENTAL RESULTS

In order to validate the theoretical assumptions, an experimental prototype was designed according the following specifications: V_{in} = 420V;V_0 = 60V;P_0 = 6kW;f_s = 46kHz.

Fig 10 shows the efficiency obtained for the proposed converter compared with other rectifier topologies [5] [6], as data were obtained in open loop situation. From this graph, it can be said that this is an intermediary solution, since efficiency is better than that in [5] but the increase in the global volume is not as large as in [6]. In Fig. 11, currents through primary windings are depicted, where a satisfactory equilibrium among them is verified (I_{Lpa}=6,3A, I_{Lpb}=5,95A, I_{Lpc}=6,6A). Fig. 12 shows line currents (I_A=10,7, I_B=10,4A, I_C=10,3A).

In Fig. 13, one can see the voltages across rectifier diodes D_4, D_5 and D_6, using an RCD snubber. Fig. 14 shows the voltages across switches S_2, S_4 and S_6.

The results above demonstrate the funcionality of the converter for $D\cong1$. However, the worst condition for disequilibrium in the output inductors i_{L01} and i_{L02} occurs when D<1. Then, Fig. 15 shows the currents through output inductors for D=0.42. This important result demonstrates the ability of this converter to control the output voltage.

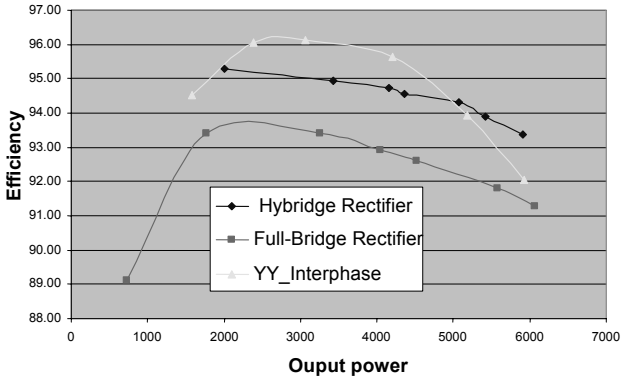

Fig. 10 – Currents through output inductors i_{L01} and i_{L02} for D=0.98 (10A/div – 10μs/div).

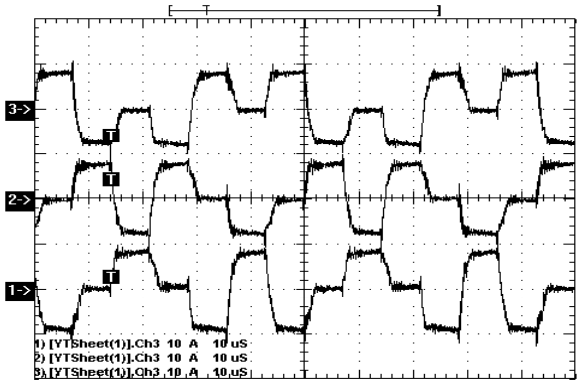

Fig. 11 – Currents through primary windings for D=0.98 (R_1 – i_{Lpa}; R_2 – i_{Lpb}; R_3 – i_{Lpc}; 10A/div).

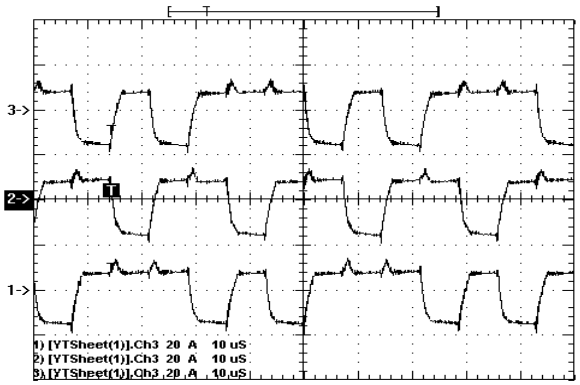

Fig. 12 –Line currents (phase C – channel 1, phase B – channel2, phase A – channel 3) (20A/div – 10μs/div).

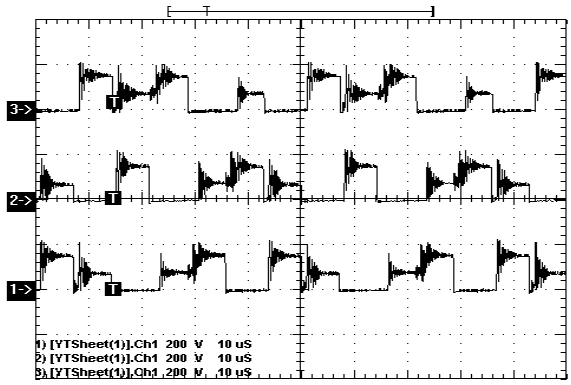

Fig. 13 – Voltage across output rectifier diodes D_4, D_5 and D_6 (200V/div – 10us/div).

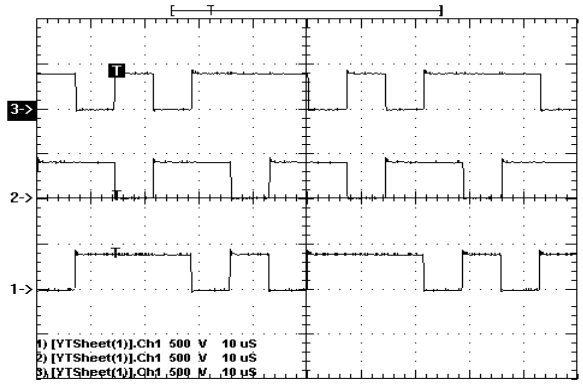

Fig. 14 – Voltage across switches S_2, S_4 and S_6 (500V/div – 10us/div).

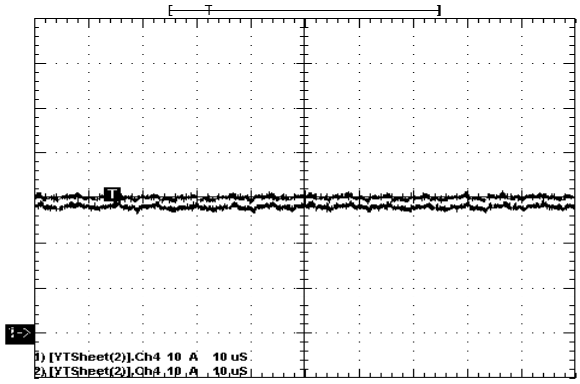

Fig. 15 – Currents through output inductors i_{L01} and i_{L02} for D=0.42 (10A/div - 10μs/div).

V. CONCLUSION

This paper has shown that the use of a three-phase dc/dc converter associated with a delta double-wye connected rectifier with interphase transformer is able to control the output voltage. In order to maintain the equlibrium, PN modulation technique was proposed.

The operating stages and main waveforms were presented and analysed. From the theoretical analysis, the cause of the disequilibrium between the output inductors current was elucidated. Then, a modulation technique was proposed and analysed. Besides, the dynamical model of the converter was obtained.

Experimental results showed that the proposed topology is an alternative for the three-phase dc/dc converter, since efficiency is better than that in full-bridge rectifier but the increase in the global volume is not as large as in hybridge rectifier.

All theoretical considerations were validated by simulation and the experimental results, obtained from a laboratory prototype of 6kW.

ACKNOWLEDGEMENT

The authors greatefully acknowledge CNPq and Brazilian MCT for the finantial support.

REFERENCES

[1] I. Barbi, W.A. Filho, “A Non-Resonant Zero Voltage Switching Pulse Width Modulated Full-Bridge DC/DC Converter,” *in Proc. IECON*, pp. 1051-1056, 1990.

[2] R.L. Steigerwald, K.D.T. Ngo, “Full-Bridge Lossless Switching Converter,” *U.S. Patent 4864479*, Sept 5, 1989.P.D. Ziogas, A.R. Prasad, S. Manias, “Analysis and Design of A Three-Phase Off-Line DC/DC Converter with High Frequency Isolation,” *in Proc IAS*, pp. 813-820, 1988.

[3] N. Mohan, P. Imbertson, “Asymmetrical Duty Cycle Permits Zero Switching Loss in PWM Circuits With no Conduction Loss Penalty,” *IEEE Transactions on Industry Applications*, vol. 29, pp. 121-125, Jan/Feb, 1993.

[4] D.S. Oliveira Jr, I. Barbi, “A DC/DC ZVS Three-Phase Converter with Asymmetrical Duty Cycle,” *IEEE Transactions on Power Electronics*, vol. 20, pp. 370-377, Mar/Ap, 2005.

[5] D.S. Oliveira Jr, I. Barbi, “D.S. Oliveira Jr. and I. Barbi, “A Three-Phase Version of the Hybridge Rectifier Associated to the Three-Phase ZVS DC/DC Converter with Asymmetrical Duty Cycle,” *in Proc. IEEE International Symposium on Industrial Electronics*, ISIE 2003, pp. 516-520, Rio de Janeiro, Brazil, 2003.

[6] J. Schaefer, *Rectifier Circuits: Theory and Design*, John Wiley & Sons, 1965.

[7] D.S. Oliveira Jr, F.L.M. Antunes, “A Novel Modulation Technique Applied to the Three-Phase ZVS PWM DC/DC Converter Associated with A Double-Wye Connected Rectifier, Delta Primary”, *Sixth IEEE International Conference on Industrial Applications*, VI INDUSCON, October 12-15, 2004, Joinville, Brazil, pp. 852-856.

[8] D.S. Oliveira Jr., I. Barbi, “Dynamical Analysis of The Three-Phase DC/DC Converter with Asymmetrical Duty Cycle, Associated to A Three-Phase Version of The Hybridge Rectifier,” *in Proc. Brazilian Power Electronics Conference,* COBEP 2003, Fortaleza, Brazil, vol. 1, pp. 65-69, 2003.